

Article

Influence of Commercial Biochar Fillers on Brittleness/Ductility of Epoxy Resin Composites

Mattia Bartoli ^{1,*}, Mauro Giorcelli ¹, Carlo Rosso ², Massimo Rovere ¹, Pravin Jagdale ³
and Alberto Tagliaferro ^{1,4}

¹ Department of Applied Science and Technology, Polytechnic University of Turin, Corso Duca degli Abruzzi 24, 10129 Turin, Italy

² Department of Mechanical and Aerospace Engineering, Polytechnic University of Turin, Corso Duca degli Abruzzi 24, 10129 Turin, Italy

³ Center for Sustainable Future, Italian Institute of Technology, Via Livorno 60, 10144 Turin, Italy

⁴ Faculty of Science, University of Ontario Institute of Technology, 2000 Simcoe Street North, Oshawa, ON L1G 0C5, Canada

* Correspondence: mattia.bartoli@polito.it; Tel.: +39-011097348

Received: 3 July 2019; Accepted: 30 July 2019; Published: 1 August 2019



Abstract: Production of versatile composites is a very attractive field. Carbon containing epoxy resins are one of the most relevant reinforced plastics used for a wide number of applications. In this research, we studied the influence of five different commercial biochar samples for the selective enhancement of brittleness and ductility of an epoxy based composite. We proved the relationship between biochar morphology and composites mechanical properties with the aid of FT-IR and FE-SEM analysis. We were able to improve the neat resin mechanical properties by doubling its Young's modulus and ultimate tensile strength using a wheat straw derived material, and to increase its elongation by 40%, we used a *Miscanthus* derived biochar.

Keywords: biochar; epoxy resin; mechanical properties; pyrolysis; reinforced polymer

Highlights

- Ultrasonication based procedure was developed to easily disperse biochar into epoxy matrix;
- Using wheat straw derived biochar as a filler, the Young's modulus doubles that of neat epoxy resin;
- Using a *Miscanthus* derived biochar, an increment of 40% of the maximum elongation value is obtained;
- A relationship between biochar and composites brittleness/ductility is found and an interpretative model was proposed.

1. Introduction

Epoxy composites field has been deeply investigated because of its common use in several manufactory processes [1]. They play a main role in both aviation and automotive sectors [2,3]. The combination of epoxy matrix with nanostructured carbonaceous fillers (i.e., CNTs, carbon fibers, graphene) is one of the most investigated approaches used for high performance materials production [4,5]. Despite their astonishing properties, the production of nanostructured carbon composites involves some unavoidable and rather critical issues. The most relevant is merely economic and it is due to the high price of the fillers for CNTs that can be as high as thousands of €/kg. Furthermore, nanostructured carbon is not easily dispersible as reported by many authors neither in epoxy resins [6] nor in thermoplastic matrices [7]. Among carbonaceous fillers, a non-traditional sustainable alternative is represented by the carbon residue of biomasses pyrolysis known as biochar [8].

As recently reported by Khan et al. [9,10], biochar could be used as replacement for traditional high performance carbon fillers such as CNTs. Furthermore, biochars with different thermal histories lead to different properties of the epoxy composites [11]. Moreover, Das et al. [12] enlighten the relationship between different feedstocks and the mechanical properties of biochar. In a further study, Das et al. [13] tested biochar from different feedstocks in a polypropylene matrix showing an appreciable improvement of tensile and flexural properties. Despite these promising properties, biochar production is generally limited to small scale or not reproducible batch after batch. The poor reproducibility has many causes such as the quality of the feedstock and the process parameters. In this article, we reported a study about the incorporation of commercial standardized biochars derived from various feedstocks into an epoxy matrix. The high reproducibility of biochar batches grants the availability of larger amounts of standard materials. Furthermore, the variety of the feedstock used allows us to select the appropriate material for each task. In this study, we correlate the changes in brittleness and ductility of biochar-based composites with the morphological properties of the carbonaceous filler used. A hypothetical interaction mechanism is also proposed.

2. Materials and Methods

2.1. Materials

Commercial standardized biochars were purchased from UK Biochar Research Centre. Chosen samples were produced from five different biomasses feedstock (*Miscanthus*, wheat straw, oil seed rape, rice husk, and mixed softwoods) using a pilot-scale rotary kiln pyrolysis unit [14] setting the highest treatment temperature (HTT) to 550 °C. Pyrolysis parameters and yields are summarized in Table 1 according to the producer data (further info on the feedstock can be found following the link in reference [15]).

Table 1. Main pyrolytic process parameters adopted by UK Biochar Research Centre for the production of standardized biochar samples.

Feedstock	ID	Heating Rate (°C/min)	Residence Time (min)		Biochar Yield (wt.%)
			Kiln Residence Time	HTT Residence Time	
<i>Miscanthus</i> straw	MSP	65	12	4	22.8
Wheat straw	WSP	80	15	5	24.1
Rice husk	RH	98	15	8	37.2
Mixed softwoods	SWP	78	12	4	21.8
Oil seed rape	OSR	78	12	5	28.9

Two components BFA diglycidyl resin were purchased from CORES (Cores epoxy resin, LPL). The curing agent was a mix of primary amines and DMP-30 promoting a two steps polymerization process (see with Figure 1).

In the first step of polymerization, epoxy groups reacted with amines at room temperature producing a low polymerization degree material with aromatic or aliphatic inter chains junction. Afterwards, a thermal curing was carried out to complete the polymerization. During both steps, DMP-30 acted as catalyst and co-curing agent promoting a more uniform polymerization process. Use of small chains amines (1,3-phenylenedimethanamine and N¹,N³-dimethylpropane-1,3-diamine) together with the presence of residual hydroxylic functionalities made this material of interest for plenty of applications, such as casting or lamination [16].

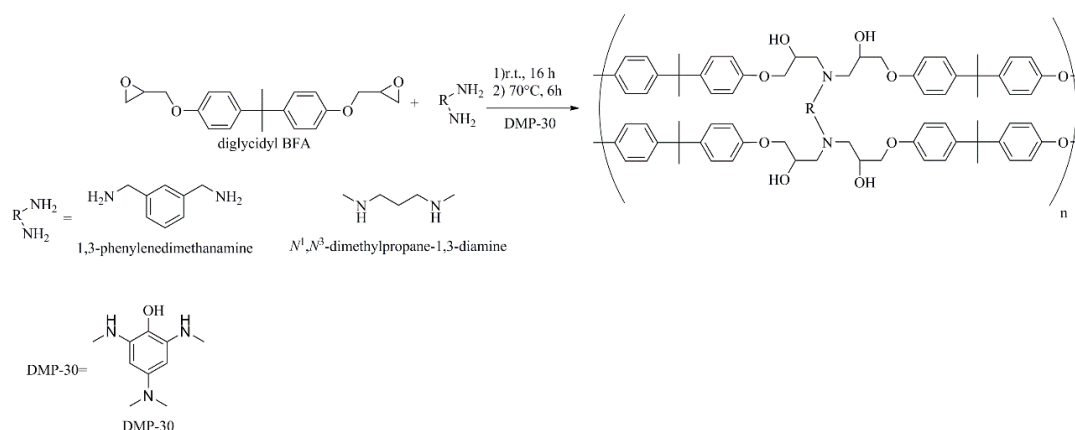


Figure 1. Polymerization process of epoxy resin with secondary amine based curing agent.

2.2. Methods

Proximate, ultimate, and surface analysis were run by UK Biochar Research Centre (School of Geosciences, University of Edinburgh, Kings Buildings, Edinburgh, EH9 3JN Scotland, UK) and reported in the datasheets of the biochars [15]. Analysis showed the high reproducibility of the materials.

The morphology of biochars was investigated using a Field Emission Scanning Electron Microscope (FE-SEM, Zeis SupraTM 40).

Biochars were also analyzed in the range from 500 cm^{-1} to 4000 cm^{-1} using a Fourier transformed infrared (FT-IR) spectrometer (Nicolet 5700, Thermoscientific, Waltham, MA, US) operated in attenuated total reflectance (ATR) equipped with a diamond window (Smartorbit, Thermoscientific, Waltham, MA, US)).

Raman spectroscopically analysis was carried out using Renishaw[®] Ramanscope InVia (H43662 model, Renishaw, Gloucestershire, UK).

To prepare composites, biochars were mechanically pulverized and subsequently dispersed into the epoxy monomer using a tip ultrasonicator apparatus (Sonics Vibra-cell) for 15 min.

Particle size distribution was evaluated using a laser granulometry (Fritsch Analysette 22, Idar-Oberstein, Germany) after dispersion in ethanol and sonication in an ultrasonic bath for 10 min.

Ultrasonication has been proven as a very effective method to realize well dispersed suspensions of CNTs in water [17] or polymeric media [18]. Despite the good performances, ultrasonication could induce disruptive phenomena due to ultracavitation effect with localized hot spot up to a thousand °C [19]. In order to avoid the instantaneous temperature rise, ultrasounds were pulsed with cycles of 20 s alternating to pause of 10 s to allow a better heat diffusion. After the addition of the curing agent, the mixture was further ultrasonicated for 2 min and left into the moulds for 16 h at room temperature. A final thermal curing was performed using a ventilated oven (I.S.C.O. Srl “The scientific manufacturer”) at 70 °C for 6 h.

Biochar containing composites were produced in dog-bone shape according with ASTM 638 procedure. Samples were tested using a MTS machine (MTS Q-test10). Data were analyzed using a homemade software compiled using Matlab[®]. Average values of at least three samples were reported.

3. Results

3.1. Biochars Characterization

A summary of the biochars physiochemical properties of interest in the present research is reported in Table 2.

Table 2. Main chemical and physical properties of biochar samples.

ID	Proximate Analysis (wt.%)				Ultimate Analysis (%)				Specific Surface Area (m ² /g)
	Moisture	Ash	VOCs	Fixed Carbon ^a	C	H	N	O ^b	
MSP	1.83	12.15	11.62	74.40	75.41	2.42	0.78	9.24	33.6
WSP	1.68	10.55	21.25	66.52	68.26	2.10	1.39	6.92	26.4
RH	1.54	47.93	7.48	43.05	48.49	1.24	1.04	2.47	20.1
SWP	1.52	1.25	14.20	83.03	85.53	2.77	0.10	10.36	26.4
OSR	2.61	19.50	16.38	61.51	68.85	1.82	1.59	8.91	7.3

^a Calculated as difference, ^b calculated as difference considering the ash content.

Using the same HTT and similar residence times, the differences in the properties of biochars are due to the differences of the feedstocks [20] as clearly evidenced by TGA, ultimate and proximate analysis [14]. Rice husk (RH) showed a remarkably high ash content, up to 47.93 wt.%, with the ash mainly composed by silica [21]. Oil seed rape (OSR) ash content was particularly high (19.50 wt.%) according to Orlovius et al. [22], while *Miscanthus* straw (MSP) and wheat straw (WSP) ash content close to 10 wt.%. Mixed softwood (SWP) ash content was the lowest: 1.25 wt.%. Carbon percentages of WSP and OSR were similar (68.26 wt.% and 68.86 wt.%, respectively), while higher carbon contents were found for MSP and SWP (75.41 wt.% and 85.53 wt.%, respectively). In agreement with its high ash content, RH showed a low carbon content: 48.49 wt.%. Nitrogen content was generally between up to 1 wt.% with the exception of MSP and SWP that showed very low values (0.78 wt.% and 0.10 wt.%, respectively).

Specific surface area values of RH, WSP, and RH were all close of up to 20 m²/g while MSP and OSR had higher and lower values, respectively (33.6 and 7.3 m²/g, respectively).

The trend of surface area values can be understood looking at the FE-SEM captures shown in Figure 2.

According to Figure 2c,d, OSR showed the presence of pores and quasi-collapsed channels filled with small carbon particles (average size below 1 µm) that sensibly reduced the overall available area. MSP showed a similar behavior but, as clearly reported in Figure 2b, the 3 to 4 µm wide channels were generally empty and filled with particles only after damage occurred. Open and diffuse channels were present in WSP together with small round shaped inter-channels pores. Inter-channels pores represented a proper wood structure and they became more relevant after pyrolytic treatments [9,23]. According to its softwood original structure [24], SWP showed a very clean surface with isolated pores having an average diameter of 2 µm (Figure 2g). RH showed a very interesting morphology with the presence of an external core covered by spikes (Figure 2e) enveloping a honeycomb structure (Figure 2f) with an average size around 1 µm and wall thickness around 700 nm.

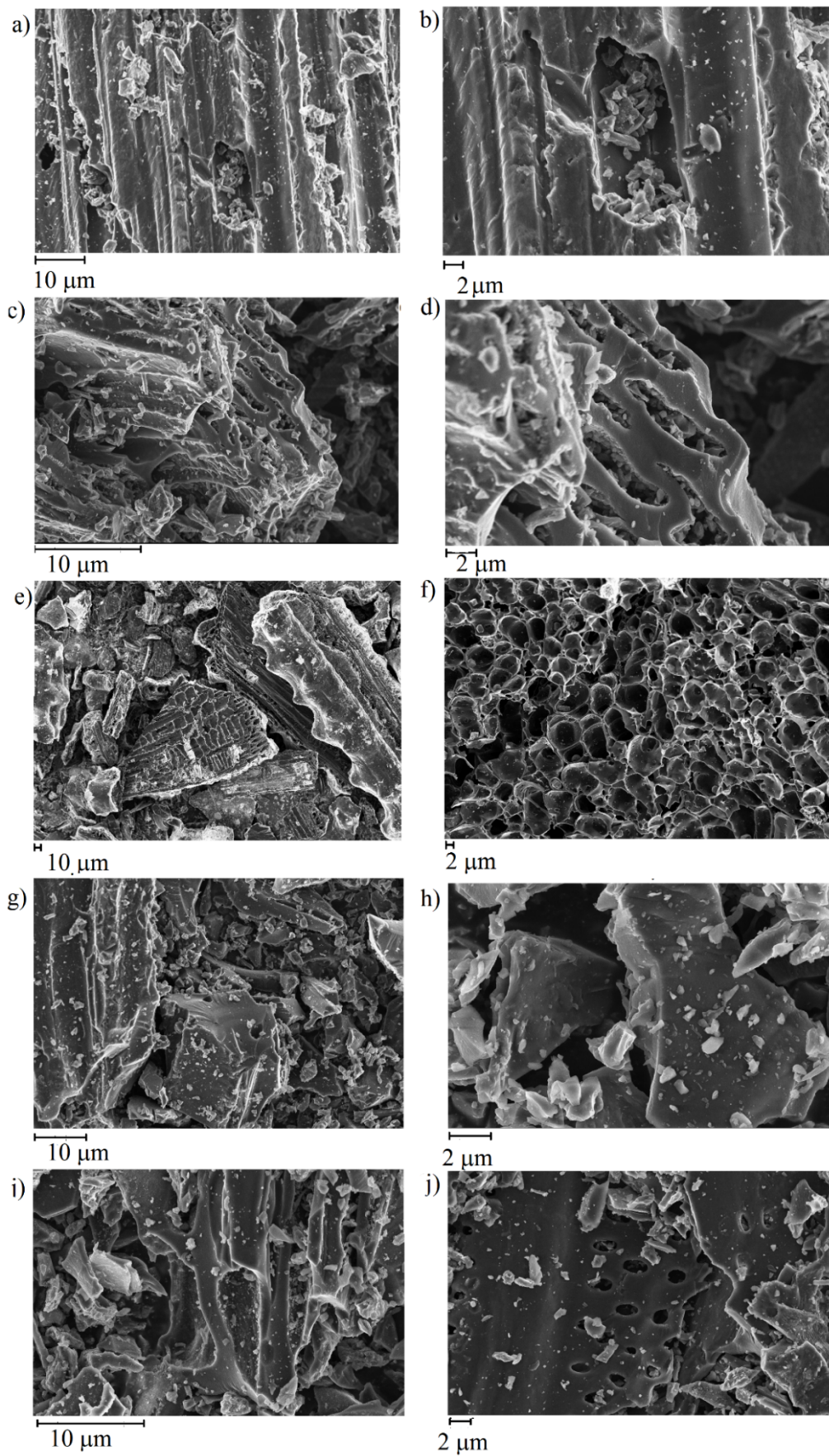


Figure 2. FE-SEM captures of (a,b) *Miscanthus* straw (MSP), (c,d) oil seed rape (OSR), (e,f) rice husk (RH), (g,h) mixed softwood (SWP), and (i,j) wheat straw (WSP).

Biochars were also analyzed by FT-IR in ATR mode and spectra were reported in Figure 3.

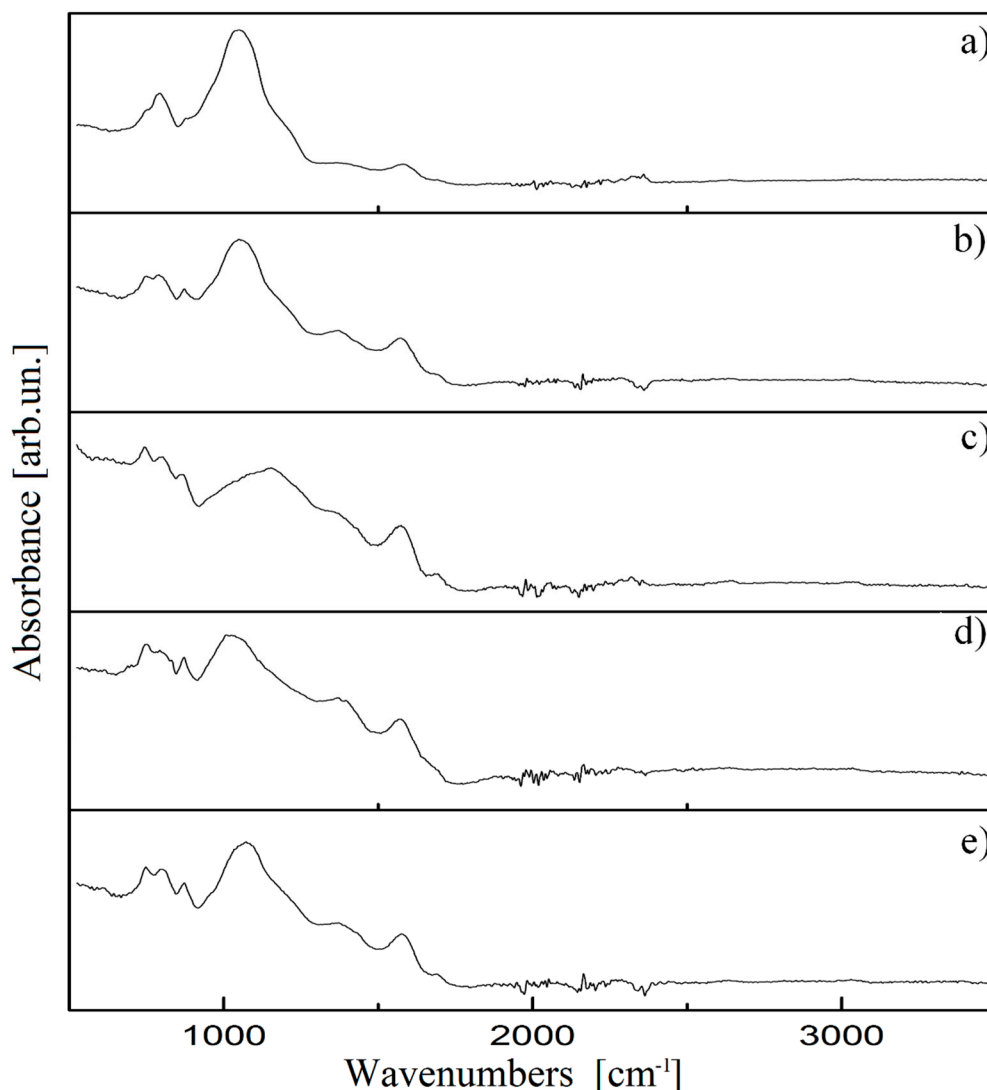


Figure 3. FT-IR attenuated total reflectance (ATR) mode spectra of (a) RH, (b) MSP, (c) SWP, (d) OSR, and (e) WSP in the region between 500 cm⁻¹ to 3500 cm⁻¹.

$\nu_{\text{O-H}}$ (3000–3500 cm⁻¹) and $\nu_{\text{C-H}}$ (2850–2900 cm⁻¹) bands were not detected in the samples in agreement with the low amount of hydrogen and oxygen (Table 2). The spectral region between 1000 cm⁻¹ and 2000 cm⁻¹ provides more detailed information about the residual functionalities of the biochars. All spectra evidenced a broad weak band around 1690 cm⁻¹ ($\nu_{\text{C=O}}$) witnessing the presence of residual ketonic groups [25]. All spectra showed a medium intense $\nu_{\text{C=C}}$ band around 1580 cm⁻¹ due to aromatic structures embedded in the carbonaceous matrix. The band around 1370 cm⁻¹ ($\delta_{\text{O-H}}$) was present in all samples but it was weaker in the RH spectrum (Figure 2e). A very intense envelop of bands can be observed between 1035 cm⁻¹ and 1070 cm⁻¹ due to several vibrational modes such as $\delta_{\text{C-O}}$, $\nu_{\text{C-O}}$. This region was particularly intense in the RH spectrum probably due to the massive presence of silica which presents an active IR mode (asymmetrical $\nu_{\text{Si-O-Si}}$) in the region 1020–1110 cm⁻¹ [26]. Silica is well-known component of rice husk derived biochar as reported by many authors [27–30]. Furthermore, the great amount of silica could be imputable of low intense of RH $\delta_{\text{O-H}}$ band. This was due to –OH reduced mobility induced by strong interactions with silica groups.

In Figure 4, the Raman spectra of the biochars used in the range between 500 cm⁻¹ to 3500 cm⁻¹ are reported.

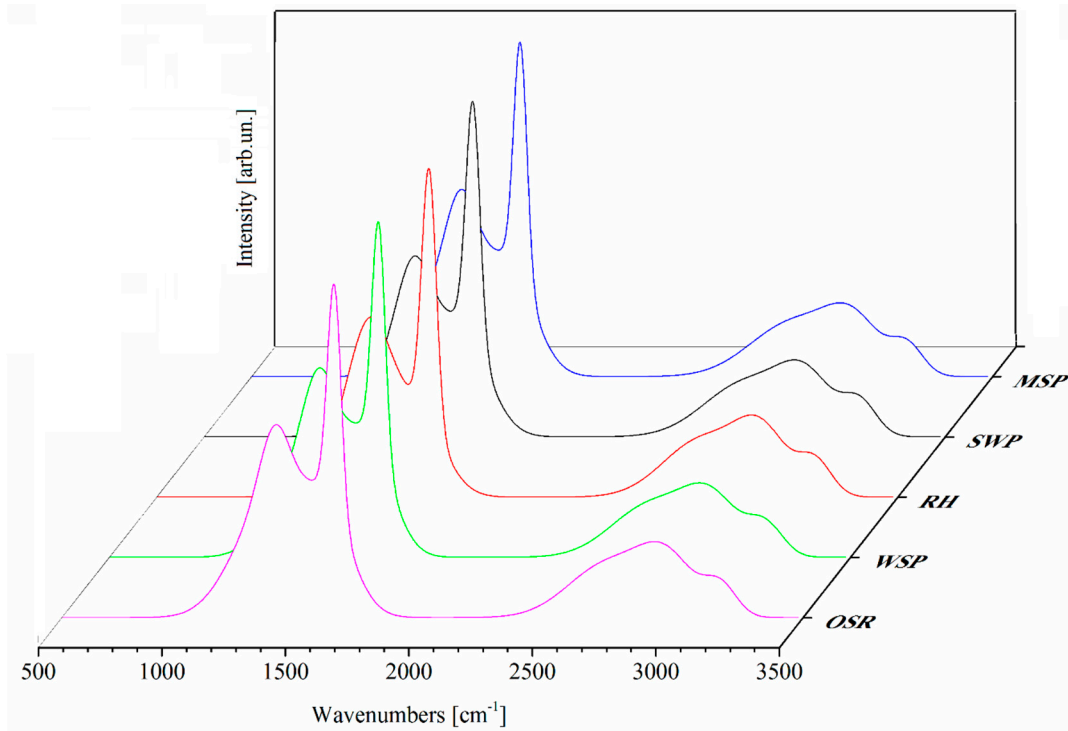


Figure 4. Raman spectra of biochars in the range between 500 cm^{-1} to 3500 cm^{-1} .

All the spectra showed two main peaks in the range 1000 to 2000 cm^{-1} currently named as D (centered around 1360 cm^{-1}) and G (centered around 1590 cm^{-1}) [31]. Less intense peaks were observed in the range between 2400 to 3300 cm^{-1} due to the overtones of the D and G peaks. According to Ferrari et al. [32], the ratio between the area of I_D and I_G peak could be used to evaluate the order of carbonaceous structures. In all the observed spectra, I_D/I_G ratios were close to each other, ranging from 1.0 (SWP) to 1.1 (RH). This was strong proof that the carbonaceous materials are equally disordered after pyrolysis. Temperature and heating rate adopted in each case were the optimum to induce the same level of molecular order in the biochar produced.

Before dispersion in polymeric matrix, biochars were mechanically grinded for 10 min and particle size distribution were analyzed. The results are reported in Figure 5.

From these results, OSR showed a particle size distribution with a large distribution centered at well-around $10\text{ }\mu\text{m}$. RH, WSP, and MSP showed the same peak at $10\text{ }\mu\text{m}$ together with a peak at a higher dimension ranging from around $50\text{ }\mu\text{m}$ to more than $100\text{ }\mu\text{m}$. SWP showed great particle size with a tailored peak centered at $100\text{ }\mu\text{m}$. The different particle distributions were a consequence of grindability of the feedstock. Considering the residual group detected in Figure 4, such distributions were due to the different morphologies formed after pyrolytic treatments [33]. According to these observations, it is possible to assume that the SWP particles were hardly grindable because of their smooth surfaces. As highlighted in Figure 2e, f, SWP did not show a channeled and porous surface as all the other materials. Accordingly, it is reasonable to assume that pore and channel walls are more fragile than smooth surfaces and undergo a more relevant disruption during the grinding process.

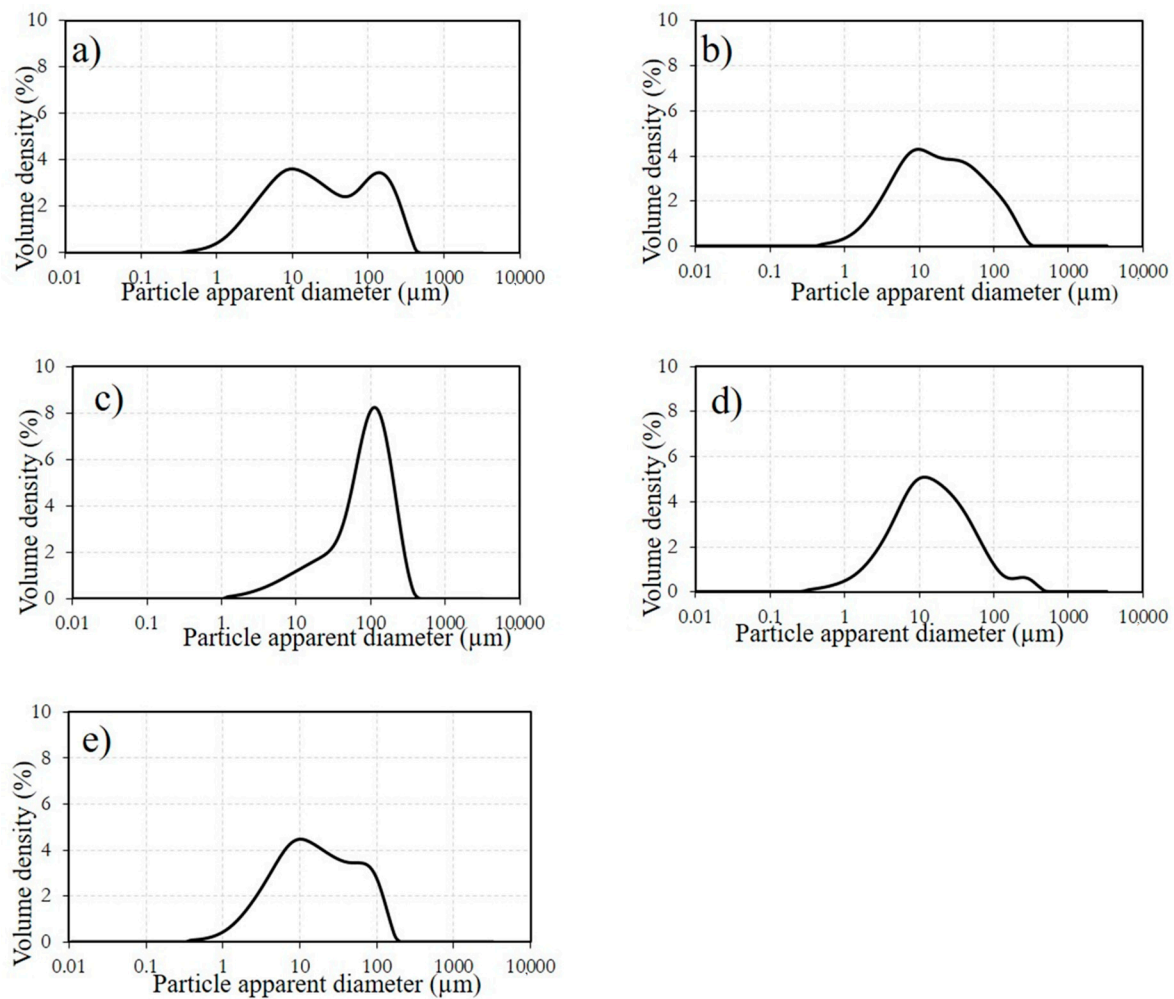


Figure 5. Biochar particles size distribution of (a) RH, (b) MSP, (c) SWP, (d) OSR, and (e) WSP after grinding.

3.2. Mechanical Properties of the Biochar-Based Composites

Addition of nanostructured carbon to an epoxy matrix involves some issues related to the dispersion [34]. As an example, good dispersion of graphene was possible only after derivatization as graphene oxide or reducing its concentration [35,36]. In this research, composites were prepared dispersing biochars into epoxy monomer using ultrasonication up to 2 wt.%. According to Khan et al. [10], 2 wt.% resulted the best percentage to exploit the beneficial properties of biochar fillers.

Dog-bone samples were produced according to the methods described above using a filler concentration of 2 wt.% and analyzed through stress test producing the curves reported in Figure 6 while the main mechanical properties are summarized in Figure 7.

Neat resin has a Young's modulus (YM) of 1286 ± 185 MPa, an ultimate tensile strength (UTS) of 17.0 ± 1.4 MPa, a maximum elongation of $4.08 \pm 0.08\%$, and a toughness of 0.565 ± 0.029 MJ/m³. Composites showed two different behaviors leading either to the simultaneous increment of UTS and YM, or to the enhancement of maximum elongation with lesser impact on YM and UTS. OSR and WSP induced a drastic increase of YM (up to 2731 ± 113 MPa and 3074 ± 137 MPa, respectively) and UTS up to around 33 MPa. Compared with these last two samples, MSP and SWP showed lower YM (1669 ± 89 MPa and 1456 ± 79 MPa, respectively) and UTS did not significantly differ from neat resin. Differently, MSP and SWP induced a maximum elongation increment of up to 1.8% compared with the neat resin, while OSR and WSP decreased it to $2.46 \pm 0.08\%$ and $1.90 \pm 0.44\%$, respectively. Compared to the properties of OSR or WSP composites, RH composite showed lower improvement of YM of up to

2166 ± 129 MPa with a comparable maximum elongation of 2.70 ± 0.14%. According with data reported in Table 2, it is possible to regroup the composites in brittle (OSR, WSP, and RH) characterized by both high YM and UTS and ductile (MSP and SWP) with improved elongation. These different behaviors could be ascribed to different interactions between fillers and epoxy matrix. According to FT-IR spectra (Figure 3), all biochars showed similar residual groups, but looking at FES-SEM images (Figure 2), we found clear differences among the various fillers. Furthermore, the particle size distributions were quite close to each other, with exception of RH, to induce such different behaviors. Based on such evidences, we hypothesized the following explanation for the impact of the fillers on the mechanical properties of the composites. Considering SWP and MSP, neat or slightly channeled surface particles (Figure 1a,b,g,h) could move together with the resin under longitudinal stress. This could induce plane rearrangement and a quasi-laminar flow with an increase in ductility. On the other hand, OSR and WSP showed the massive presence of pores that can act as anchoring sites for the polymer matrix creating high tensioned structures. As a consequence, these materials showed lower yield points and plastic deformation range prior to the breakage than neat resin. Composites were analyzed through FE-SEM after fracture as shown in Figure 8. MSP containing composites underwent a delamination process after the break. In this case, resin was detached from the channel structures (Figure 8a,b in white circles). OSR based composites showed a different behavior. As shown in Figure 8c,d, the resin entirely filled the OSR porous structure showing a remarkably continuity on the interphases. In this case, cracks propagated themselves all around the particles while using MSP they moved preferentially along the channeled structures.

Additional considerations were required in the case of RH based composites that showed both plane surfaces and spikes and pores. This combination was detrimental for the ductility and this fact suggests the more relevant role of brittleness inducing elements on the ductility inducing ones.

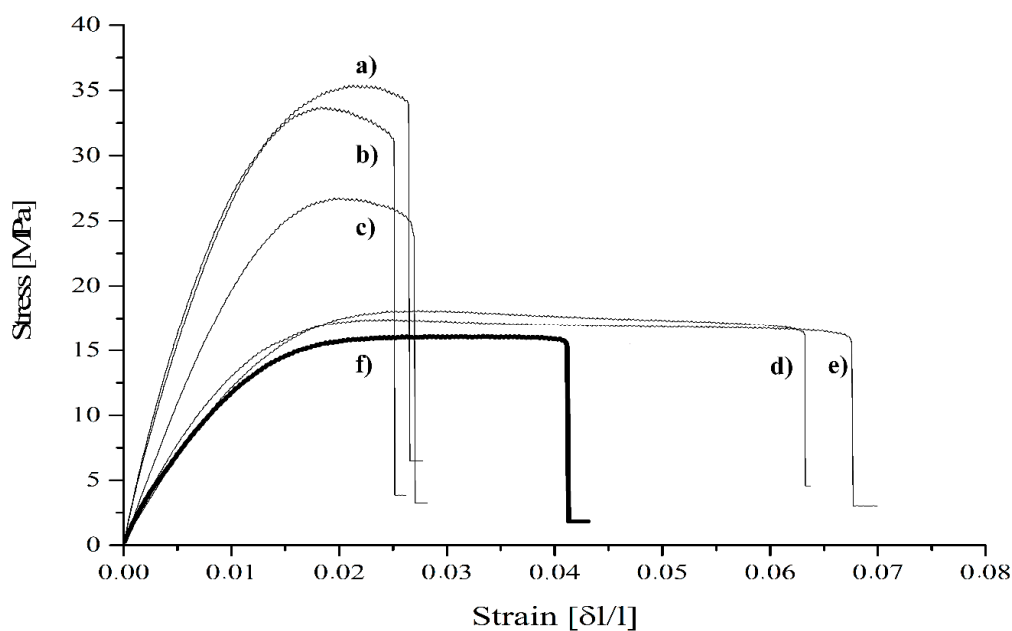


Figure 6. Stress versus strain curves of biochar-based composites filled with 2 wt.% of (a) WSP, (b) OSR, (c) RH, (d) SWP, (e) MSP, and of (f) neat resin.

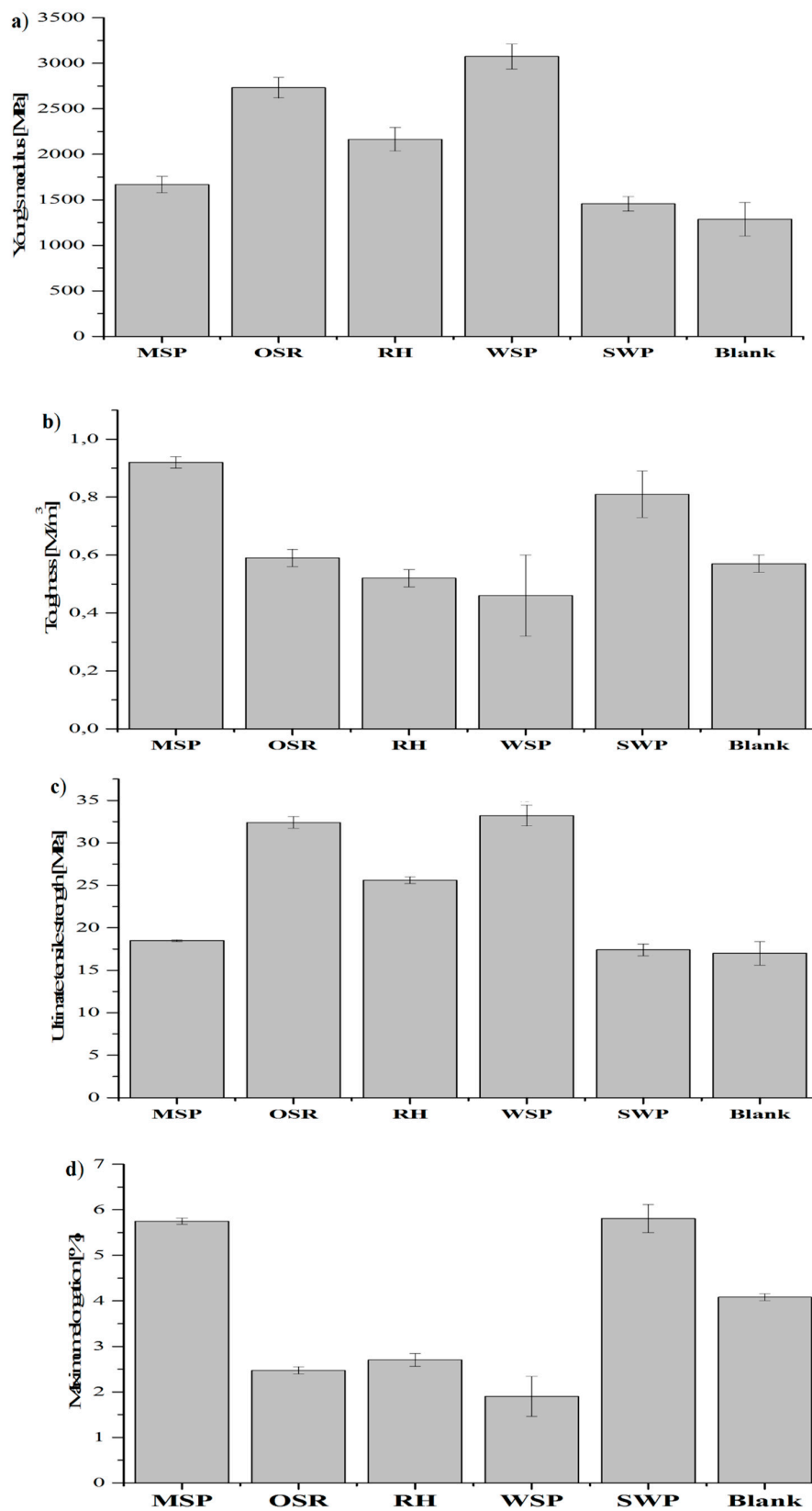


Figure 7. (a) Young's modulus, (b) toughness, (c) ultimate tensile strength, and (d) maximum elongation of biochar containing composites and neat resin. Data were reported as average values of at least three runs.

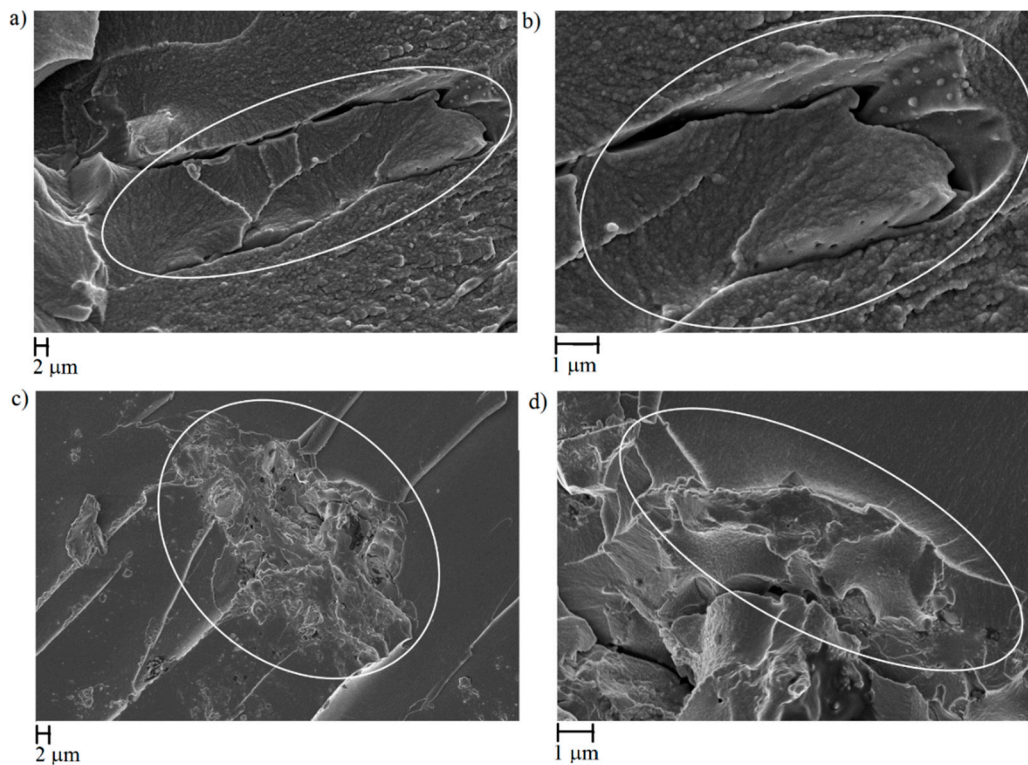


Figure 8. FE-SEM captures of composites containing (a,b) MSP and (c,d) WSP after the fracture. FE-SEM. Interphases between biochar particles and resin are highlighted with white circles.

4. Conclusions

In this research, the properties of five different commercial biochars were analyzed and their main morphological aspects were reported. Biochar were dispersed into an epoxy matrix through an ultrasonication method and mechanical properties were tested. MSP and SWP showed the best elongation performances with appreciable improvement of the ductility compared with neat resin. OSR, WSP, and RH induced a drastically decrease of the ductility with a magnification of Young's modulus and ultimate tensile strength. Considering the similar residual groups detected through FT-IR analysis, mechanical properties could be ascribed to the different biochar morphologies and not to the particle size distribution. Channeled and smooth surfaces induced improvement in ductility contrary to high porous and irregular surfaces that promote higher brittleness.

Author Contributions: Conceptualization: M.B. and A.T.; methodology: M.B., P.J., and C.R.; software: M.R.; formal analysis: M.B.; investigation: M.B.; resources: A.T.; C.R. data curation: M.B. and M.R.; writing—original draft preparation: M.B.; writing—review and editing, M.G. and A.T.; supervision: A.T.; project administration: A.T.; funding acquisition: A.T.

Acknowledgments: Authors acknowledge Andrea Marchisio's help in the particles distribution analysis, and Salvatore Guastella and Mauro Raimondo's help in FE-SEM analysis.

Conflicts of Interest: The authors declare no conflict of interest.

References

1. Jin, F.L.; Li, X.; Park, S.J. Synthesis and application of epoxy resins: A review. *J. Ind. Eng. Chem.* **2015**, *29*, 1–11. [[CrossRef](#)]
2. Friedrich, K.; Almajid, A.A. Manufacturing aspects of advanced polymer composites for automotive applications. *Appl. Compos. Mater.* **2013**, *20*, 107–128. [[CrossRef](#)]
3. Chatterjee, B.; Bhowmik, S. Evolution of Material Selection in Commercial Aviation Industry—A Review. In *Sustainable Engineering Products and Manufacturing Technologies*; Elsevier BV: Amsterdam, The Netherlands, 2019; pp. 199–219.

4. Allaoui, A. Mechanical and electrical properties of a MWNT/epoxy composite. *Compos. Sci. Technol.* **2002**, *62*, 1993–1998. [[CrossRef](#)]
5. Naebe, M.; Wang, J.; Amini, A.; Khayyam, H.; Hameed, N.; Li, L.H.; Chen, Y.; Fox, B. Mechanical Property and Structure of Covalent Functionalised Graphene/Epoxy Nanocomposites. *Sci. Rep.* **2014**, *4*, 4375. [[CrossRef](#)] [[PubMed](#)]
6. Song, Y.S.; Youn, J.R. Influence of dispersion states of carbon nanotubes on physical properties of epoxy nanocomposites. *Carbon* **2005**, *43*, 1378–1385. [[CrossRef](#)]
7. Lahelin, M.; Annala, M.; Nykänen, A.; Ruokolainen, J.; Seppälä, J. In situ polymerized nanocomposites: Polystyrene/CNT and Poly (methyl methacrylate)/CNT composites. *Compos. Sci. Technol.* **2011**, *71*, 900–907. [[CrossRef](#)]
8. Downie, A.; Crosky, A.; Munroe, P. Physical Properties of Biochar. In *Biochar for Environmental Management: Science and Technology*; Earthscan Publications Ltd.: London, UK, 2009; pp. 13–32.
9. Khan, A.; Savi, P.; Quaranta, S.; Rovere, M.; Giorcelli, M.; Tagliaferro, A.; Rosso, C.; Jia, C.Q. Low-Cost Carbon Fillers to Improve Mechanical Properties and Conductivity of Epoxy Composites. *Polymers* **2017**, *9*, 642. [[CrossRef](#)]
10. Khan, A.; Jagdale, P.; Rovere, M.; Nogués, M.; Rosso, C.; Tagliaferro, A. Carbon from waste source: An eco-friendly way for strengthening polymer composites. *Compos. Part B Eng.* **2018**, *132*, 87–96. [[CrossRef](#)]
11. Giorcelli, M.; Khan, A.; Pugno, N.M.; Rosso, C.; Tagliaferro, A. Biochar as a cheap and environmental friendly filler able to improve polymer mechanical properties. *Biomass Bioenergy* **2019**, *120*, 219–223. [[CrossRef](#)]
12. Das, O.; Sarmah, A.K.; Bhattacharyya, D. Structure–mechanics property relationship of waste derived biochars. *Sci. Total. Environ.* **2015**, *538*, 611–620. [[CrossRef](#)]
13. Das, O.; Sarmah, A.K.; Bhattacharyya, D. A sustainable and resilient approach through biochar addition in wood polymer composites. *Sci. Total Environ.* **2015**, *512*, 326–336. [[CrossRef](#)] [[PubMed](#)]
14. Mašek, O.; Buss, W.; Roy-Poirier, A.; Lowe, W.; Peters, C.; Brownsort, P.; Mignard, D.; Pritchard, C.; Sohi, S. Consistency of biochar properties over time and production scales: A characterisation of standard materials. *J. Anal. Appl. Pyrolysis* **2018**, *132*, 200–210. [[CrossRef](#)]
15. UK Biochar Research Centre-Reducing and Removing CO₂ while Improving Soils: a Significant and Sustainable Response to Climate Change. Available online: https://www.biochar.ac.uk/standard_materials.php (accessed on 29 July 2019).
16. Hara, O. *Curing Agents for Epoxy Resin*; Three Bond Co., LTD.: Tokyo, Japan, 1990; Volume 32, pp. 1–10.
17. Jiang, L.; Gao, L.; Sun, J. Production of aqueous colloidal dispersions of carbon nanotubes. *J. Colloid Interface Sci.* **2003**, *260*, 89–94. [[CrossRef](#)]
18. Ramasubramaniam, R.; Chen, J.; Liu, H. Homogeneous carbon nanotube/polymer composites for electrical applications. *Appl. Phys. Lett.* **2003**, *83*, 2928–2930. [[CrossRef](#)]
19. Rae, J.; AshokKumar, M.; Eulaerts, O.; Von Sonntag, C.; Reisse, J.; Grieser, F. Estimation of ultrasound induced cavitation bubble temperatures in aqueous solutions. *Ultrason. Sonochem.* **2005**, *12*, 325–329. [[CrossRef](#)] [[PubMed](#)]
20. Grønli, M.G.; Melaaen, M.C. Mathematical Model for Wood Pyrolysis Comparison of Experimental Measurements with Model Predictions. *Energy Fuels* **2000**, *14*, 791–800. [[CrossRef](#)]
21. Masulili, A.; Utomo, W.H.; Ms, S. Rice Husk Biochar for Rice Based Cropping System in Acid Soil 1. The Characteristics of Rice Husk Biochar and Its Influence on the Properties of Acid Sulfate Soils and Rice Growth in West Kalimantan, Indonesia. *J. Agric. Sci.* **2010**, *2*, 39. [[CrossRef](#)]
22. Orlovius, K. Fertilizing for High Yield and Quality Oilseed Rape. *IPI Bull.* **2003**, *16*, 125.
23. Baltrėnas, P.; Baltrėnaitė, E.; Spudulis, E. Biochar from Pine and Birch Morphology and Pore Structure Change by Treatment in Biofilter. *Water Air Soil Pollut.* **2015**, *226*, 69. [[CrossRef](#)]
24. Plötze, M.; Niemz, P. Porosity and pore size distribution of different wood types as determined by mercury intrusion porosimetry. *Eur. J. Wood Wood Prod.* **2011**, *69*, 649–657. [[CrossRef](#)]
25. Chia, C.H.; Gong, B.; Joseph, S.D.; Marjo, C.E.; Munroe, P.; Rich, A.M. Imaging of mineral-enriched biochar by FTIR, Raman and SEM–EDX. *Vib. Spectrosc.* **2012**, *62*, 248–257. [[CrossRef](#)]
26. Feifel, S.C.; Lisdat, F. Silica nanoparticles for the layer-by-layer assembly of fully electro-active cytochrome c multilayers. *J. Nanobiotechnol.* **2011**, *9*, 59. [[CrossRef](#)] [[PubMed](#)]
27. Prakongkep, N.; Gilkes, R.J.; Wiriyakitnateekul, W.; Duangchan, A.; Darunsontaya, T. The effects of pyrolysis conditions on the chemical and physical properties of rice husk biochar. *Int. J. Mater. Sci.* **2013**, *3*, 97–103.

28. Guo, J.; Chen, B. Insights on the Molecular Mechanism for the Recalcitrance of Biochars: Interactive Effects of Carbon and Silicon Components. *Environ. Sci. Technol.* **2014**, *48*, 9103–9112. [[CrossRef](#)] [[PubMed](#)]
29. Liou, T.H.; Yang, C.C. Synthesis and surface characteristics of nanosilica produced from alkali-extracted rice husk ash. *Mater. Sci. Eng. B* **2011**, *176*, 521–529. [[CrossRef](#)]
30. James, J.; Rao, M. Silica from rice husk through thermal decomposition. *Thermochim. Acta* **1986**, *97*, 329–336. [[CrossRef](#)]
31. Merlen, A.; Buijnsters, J.G.; Pardanaud, C. A Guide to and Review of the Use of Multiwavelength Raman Spectroscopy for Characterizing Defective Aromatic Carbon Solids: From Graphene to Amorphous Carbons. *Coatings* **2017**, *7*, 153. [[CrossRef](#)]
32. Ferrari, A.C.; Robertson, J. Interpretation of Raman spectra of disordered and amorphous carbon. *Phys. Rev. B* **2000**, *61*, 14095–14107. [[CrossRef](#)]
33. Weber, K.; Quicker, P. Properties of biochar. *Fuel* **2018**, *217*, 240–261. [[CrossRef](#)]
34. Allaoui, A. How carbon nanotubes affect the cure kinetics and glass transition temperature of their epoxy composites?—A review. *Express Polym. Lett.* **2009**, *3*, 588–594. [[CrossRef](#)]
35. Stankovich, S.; Dikin, D.A.; Dommett, G.H.; Kohlhaas, K.M.; Zimney, E.J.; Stach, E.A.; Piner, R.D.; Nguyen, S.T.; Ruoff, R.S. Graphene-based composite materials. *Nature* **2006**, *442*, 282. [[CrossRef](#)] [[PubMed](#)]
36. Ramanathan, T.; Abdala, A.A.; Stankovich, S.; Dikin, D.A.; Herrera-Alonso, M.; Piner, R.D.; Adamson, D.H.; Schniepp, H.C.; Chen, X.; Ruoff, R.S.; et al. Functionalized graphene sheets for polymer nanocomposites. *Nat. Nanotechnol.* **2008**, *3*, 327–331. [[CrossRef](#)] [[PubMed](#)]



© 2019 by the authors. Licensee MDPI, Basel, Switzerland. This article is an open access article distributed under the terms and conditions of the Creative Commons Attribution (CC BY) license (<http://creativecommons.org/licenses/by/4.0/>).